Simulations of atmospheric pressure discharge in a high-voltage nanosecond pulse using the particle-in-cell Monte Carlo collision model in noble gases

Feng Shi, Dezhen Wang, and Chunsheng Ren

Articles you may be interested in

Particle-in-cell/Monte Carlo collision simulation of the ionization process of surface-wave plasma discharges resonantly excited by surface plasmon polaritons
Phys. Plasmas **20**, 033502 (2013); 10.1063/1.4794736

Studies on nanosecond pulsed atmospheric pressure discharge with particle-in-cell Monte Carlo collision simulation
Phys. Plasmas **19**, 093510 (2012); 10.1063/1.4755788

Study of applied magnetic field magnetoplasmadynamic thrusters with particle-in-cell code with Monte Carlo collision. I. Computation methods and physical processes
Phys. Plasmas **19**, 073107 (2012); 10.1063/1.4737098

Three-dimensional particle-in-cell simulation of discharge characteristics in cylindrical anode layer hall plasma accelerator
Phys. Plasmas **19**, 043507 (2012); 10.1063/1.3703321

Characteristics of nanosecond pulse needle-to-plane discharges at high pressure: a particle-in-cell Monte Carlo collision simulation
J. Appl. Phys. **105**, 043305 (2009); 10.1063/1.3082111

Simulations of atmospheric pressure discharge in a high-voltage nanosecond pulse using the particle-in-cell Monte Carlo collision model in noble gases

Feng Shi, Dezhen Wang,[a)] and Chunsheng Ren
State Key Laboratory of Materials Modification by Laser, Ion and Electron Beams, School of Physics and Optoelectronic Technology, Dalian University of Technology, Dalian 116024, People's Republic of China

Atmospheric pressure discharge nonequilibrium plasmas have been applied to plasma processing with modern technology. Simulations of discharge in pure Ar and pure He gases at one atmospheric pressure by a high voltage trapezoidal nanosecond pulse have been performed using a one-dimensional particle-in-cell Monte Carlo collision (PIC-MCC) model coupled with a renormalization and weighting procedure (mapping algorithm). Numerical results show that the characteristics of discharge in both inert gases are very similar. There exist the effects of local reverse field and double-peak distributions of charged particles' density. The electron and ion energy distribution functions are also observed, and the discharge is concluded in the view of ionization avalanche in number. Furthermore, the independence of total current density is a function of time, but not of position. © *2008 American Institute of Physics*. [DOI: 10.1063/1.2927437]

I. INTRODUCTION

Due to their practical and potential applications, atmospheric pressure discharge plasma has extensively been investigated recently.[1–7] Nanosecond pulse discharge, one of the most promising approaches to produce large-volume nonequilibrium plasma at one atmospheric pressure, had been paid more and more attention in atmospheric pressure discharge plasma research.[8–10] However, there are still a lot of questions needed to be studied further, such as the high distortion of the local field influenced by the accumulation effect of the space charges, the mechanism of electrons being sped up, and so on.

In the fields of computational plasmas and gas discharge physics, one can simulate the physical processes of discharges with different physical models,[11] such as fluid schemes,[12] kinetic methods,[13,14] or the hybrid of the fluid and kinetic models.[15] In addition, finite difference (FD) schemes coupled to the flux corrected transport (FCT),[16] as well as finite element (FE) techniques in conjunction with FCT developed by Georghiou *et al.*,[17] are also valuable algorithms, and more detailed discussion about the algorithms could be found elsewhere.[5,18,19] Yet, there are few researchers using particle-in-cell Monte Carlo collision (PIC-MCC) techniques to investigate the characteristics of atmospheric pressure discharge produced by a high-voltage nanosecond pulse, which is a promising and practical way to obtain large-volume plasma.[20,21]

In this paper, we coupled a mapping algorithm developed by Kunhardt *et al.*[22] into the PIC-MCC model, and simulated the high voltage nanosecond pulse discharge at atmospheric pressure in Ar and He gases, respectively. The results show that there exists the effects of local field reversal and the double-peak profiles of electron and ion density in the discharge plasma region, which was obtained and explained for the first time by Raizer and Shneider.[23]

II. MODEL AND INITIAL CONDITIONS

The one-dimensional (1d3v) PIC-MCC model has been adopted to investigate the characteristics of atmospheric pressure discharge generated by a high-voltage nanosecond pulse. The simulation conditions can be described as follows: the gap of the parallel planar electrodes is 1 mm, the negative pulsed voltage was applied to the cathode with the grounded anode, and the rise, plateau, and drop of the pulse is 0.5, 1.5, and 0.5 ns, respectively. In the simulations, pure Ar and He were used as the working gas, respectively. Not only were the characteristics of the atmospheric pressure discharge in noble gases analyzed, but also a comparison of the characteristics in different gases had been made in the simulations. The magnitude of the plateau voltage is set at 5000 V in Ar and 3000 V in He, respectively, so that we could obtain high density plasmas and establish the space field more intensively and rapidly in the simulations, and thus observe the effect of space field on the discharge more easily. Note that, we do not apply a higher voltage because the higher values may exceed the calculated capacity of our computers. The uniform initial space charge density, electron temperature, and ion temperature are assumed to be $10^5/\text{cm}^3$, 2 eV, and 0.026 eV, respectively. Such uniform initial plasma density can be obtained by the irradiation of ultraviolet or the afterglow of the former discharge. Here we do not consider the emission of secondary electrons because the energy of most ions is so low that few secondary electrons can be produced.

The maximum plasma density in the discharge can be up to about $5 \times 10^{13}/\text{cm}^3$ in Ar and $1 \times 10^{13}/\text{cm}^3$ in He, which is about $10^8 - 10^9$ orders of the magnitude larger than the
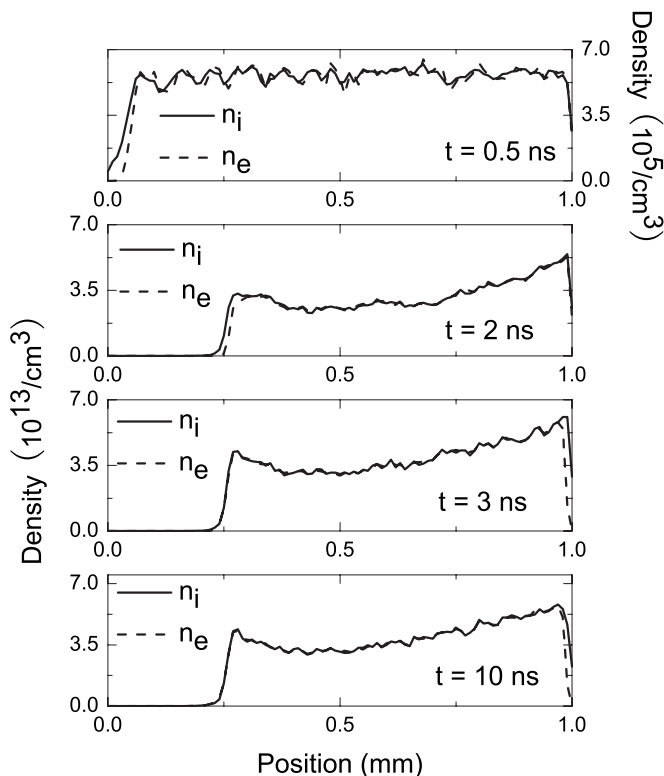

FIG. 1. Spatial and temporal profiles of electron density (n_e) and ion density (n_i) at different times in a trapezoidal high-voltage pulse with magnitude of 5000 V at one atmospheric pressure of Ar. The initial plasma density is about $10^5/cm^3$.
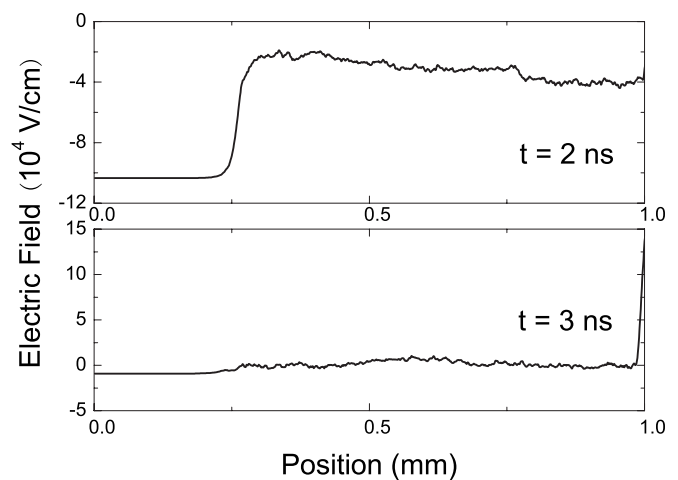

FIG. 2. Spatial and temporal profiles of the electrostatic field at $t=2$ ns and $t=3$ ns in a high-voltage pulse with magnitude of 5000 V at one atmospheric pressure of argon.

initiative due to avalanche ionization processes. Thus, in order to circumvent the limitation of particles in number that a personal computer could afford in the simulations of atmospheric pressure discharge, we have employed the mapping algorithm, also called renormalization and weighting procedure, and coupled it to the PIC-MCC model in the simulations. The mapping is accomplished by maintaining the equivalent energy distribution between the assemblies before and after the mapping, as well as the maximum resolution in the high energy tail region. More detailed discussion of the mapping algorithm is presented in Ref. 22. In the case of argon gas, the cross sections used in the MCC processes in the simulations can be found in Ref. 24. While the collision cross sections for helium, except the ones for excitation collisions of electron-neutral in Ref. 25, can be found in the Ref. 11.

III. RESULTS AND DISCUSSIONS

The spatial-temporal evolution of electron and ion densities for Ar at four different times are shown in Fig. 1, from which we can distinctly see the evolution of the sheaths and plasma volume in Ar. The maximum plasma density in the discharge can be up to about $5 \times 10^{13}/cm^3$, which is about 10^8 orders of the magnitude larger than the initiative due to avalanche ionization. The cathode sheath is much larger than the anode sheath during the pulse because we have applied a negative high-voltage pulse on the cathode. In the time scale of our interest here, about a few nanoseconds, the ions al-

most remain stationary compared to the fast electrons, so the electrons are rejected to the plasma volume which left behind the ions near the cathode. Although electrons near the anode are rapidly pulled onto the anode, the ones from plasma bulk move into that region and compensate the loss of the electrons in the anode sheath, so the cathode sheath becomes thicker and thicker than the anode sheath during the pulse as the discharge evolves, and thus a local motion-opposing space charge field to electrons begins to form as the result of the accumulation of large amounts of net ions in both sheaths. We can clearly see the evolution of high distortions of the local field from Fig. 2. At the end of the pulse, the effect of "field reversal" that usually occurs in the case of high pressure discharge due to the strong local distortion field, and the electrons near the anode are hauled back to the plasma volume by this field. Meanwhile, the space field in the cathode sheath declines, and more and more electrons can enter into the cathode region. Consequently, when the voltage pulse is over, contrary to the case during the pulse time, the cathode sheath is much thinner than the anode sheath.

There is another notable phenomenon of double-peak profile of charged particles' density, as can be seen from the spatial-temporal evolution of the discharge profiles in Ar. This illustrates that the electrons accelerated in the sheaths are drawn out of the sheaths rapidly and ionization collisions occur in the plasma volume. Furthermore, because ions are almost motionless compared to fast movement electrons in the time scale of our interest here (a few nanoseconds), the ion density profile almost remains unchanged and forms a positive background, but the strong local field greatly affects the behaviors of the electrons such as the evolution of the cathode and anode sheath, as shown in Fig. 1.

The evolution of space averaged electron energy distribution function (EEDF) between electrodes in Ar at different times is given in Fig. 3, from which we can conclude that the electrons in the high energy tail region can be speeded up above the threshold energy of ionization and cause intense avalanche ionization effects during the discharge. However,
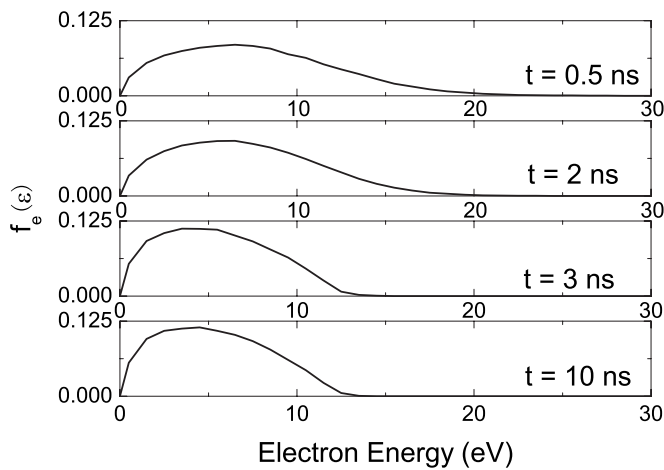
FIG. 3. Evolution of the space averaged electron energy distribution function $f_e(\varepsilon)$ between electrodes at different times in argon.

FIG. 5. The evolutions of the current densities along the discharge gap at four different times: (a), (b), (c) 0.5 ns; (d), (e), (f) 2 ns; (g), (h), (i) 3 ns; and (j), (k), (l) 10 ns. (a), (d), (g), (j) electron current density j_e; (b), (e), (h), (k) ion current density j_i; (c), (f), (i), (l) displacement current density j_d.

when the pulse is over, the energetic electrons lose energy rapidly due to the small mean free path, so the high energy tail of the EEDF decays quickly.

The evolution of space averaged ion energy distribution function (IEDF) between electrodes in Ar at different times is given in Fig. 4, from which we can clearly see that the energy of most ions in the discharge remains the room temperature. In other words, the plasma generated by nanosecond pulse is nonequilibrium plasma. That is to say, we can obtain the large-volume nonequilibrium plasma in such a manner.

Figure 5 shows us the evolution of current densities along the discharge gap at four different times. The electrons can almost immediately response the applied field, so the electron current density increases significantly as the discharge develops, shown in Figs. 5(a) and 5(d). Due to the avalanche ionization processes, the electron current density also increases drastically along the discharge gap at a given time during the discharge, as shown in Fig. 5(d). After the pulse, the electrons drift toward the both electrodes, so there appears both positive and negative electron current density in plasma volume, shown in Figs. 5(g) and 5(j). But this is not
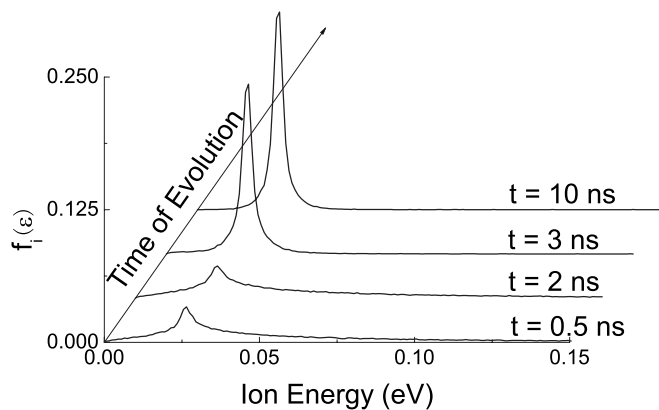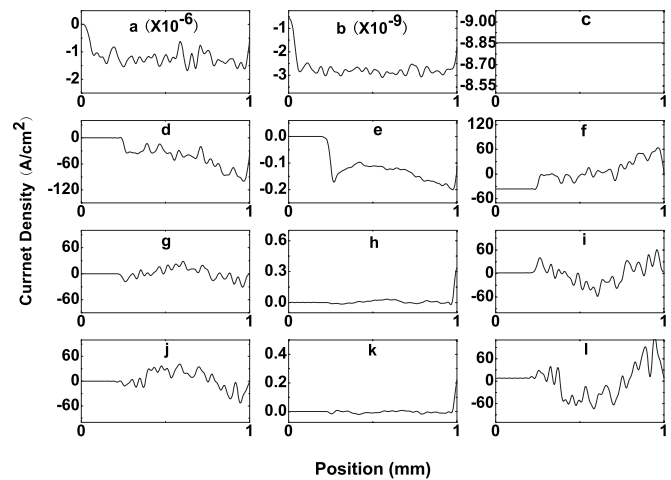
the case for the ions. As illustrated in Fig. 4, the applied pulse is such a short period that the ions can hardly gain energy from the applied field, so the ion current density is aroused only by the avalanche ionization effect during the pulse, shown in Figs. 5(b) and 5(e). When the pulse is over, since no further ionization occurs in the bulk plasma, the ion current density becomes small except in the anode region where the strong local reverse field can accelerate the ions, and because of the smaller mobility of the ions, this strong reverse field can sustained for a considerable time, shown in Figs. 5(h) and 5(k). In addition, the drastically changing field could cause a strong displacement current density, shown in Figs. 5(c), 5(f), 5(i), and 5(l). During the discharge, the displacement current density caused by the changing field mainly stems from the avalanche ionization processes. At the end of the pulse, the displacement current density becomes positive in the region where the reverse field appears, shown in Fig. 5(f). However, after the pulse, the changing field is
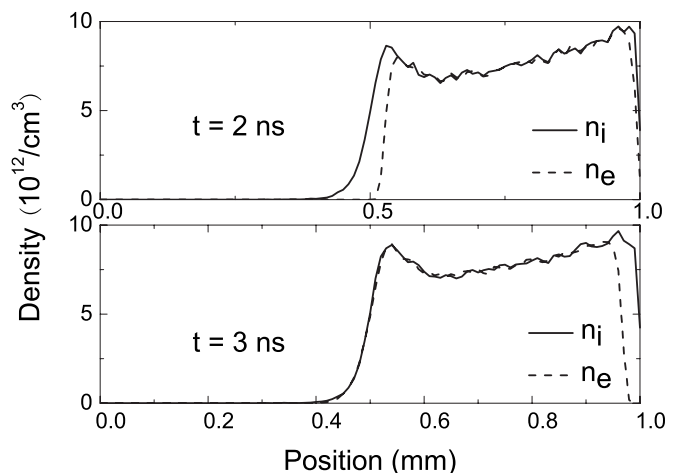

FIG. 4. Evolution of the space averaged ion energy distribution function $f_i(\varepsilon)$ between electrodes at different times in argon.

FIG. 6. Spatial and temporal profiles of electron density (n_e) and ion density (n_i) at different times in a trapezoidal high-voltage pulse with magnitude of 3000 V at one atmospheric pressure of He. The initial plasma density is about $10^5/cm^3$.

mainly caused by the electrons' drifting motions. Also from Fig. 5, we can see the total current density along the discharge gap is dependent on time and independent of position.

Similar results have been obtained from the simulations with He, as shown in Fig. 6. Our simulations have shown that stable discharge can be achieved more easily in He than in Ar due to different discharge related processes here. Thus, the magnitude of the pulse plateau about 3000 V is high enough to obtain a rapidly established space field and large-volume plasma in the simulations with He.

IV. CONCLUSIONS

In this paper, we have presented some simulation results of the characteristics of atmospheric pressure discharge produced by a high-voltage nanosecond pulse with one-dimensional planar electrode configuration in both Ar and He using the 1d3v PIC-MCC model coupled with a renormalization and weighting procedure. From these results, we can clearly see the growth of plasma density during the discharge due to the avalanche ionization. The effect of local field reversal is particularly observed at the end of the pulse. Moreover, the double-peak profile phenomenon of charged particles' density during a pulse is also predicted in our simulations. With the PIC-MCC model, we also obtain the EEDF and IEDF at different discharge times. Besides, the total current density along the discharge gap is a function of time. In our simulations, it is concluded that large-volume nonequilibrium plasma can be achieved with the nanosecond pulse.

[1]J. R. Roth, Phys. Plasmas **10**, 2117 (2003).
[2]Y.-B. Guo and F. C.-N. Hong, Appl. Phys. Lett. **82**, 337 (2003).
[3]L. Baars-Hibbe, P. Sichler, C. Schrader, C. Gessner, K. H. Gericke, and S. Buttgenbach, Surf. Coat. Technol. **174**, 519 (2003).
[4]E. E. Kunhardt, IEEE Trans. Plasma Sci. **28**, 189 (2000).
[5]G. E. Georghiou, A. P. Papadakis, R. Morrow, and A. C. Metaxas, J. Phys. D **38**, R303 (2005).
[6]U. Kogelschatz, IEEE Trans. Plasma Sci. **30**, 1400 (2002).
[7]S. Kanazawa, M. Kogoma, T. Moriwaki, and S. Okazaki, J. Phys. D **21**, 838 (1988).
[8]M. Baeva, H. Gier, A. Pott, J. Uhlenbusch, J. Höschele, and J. Steinwandel, Plasma Chem. Plasma Process. **21**, 225 (2001).
[9]V. F. Tarasenko, Appl. Phys. Lett. **88**, 081501 (2006).
[10]J. L. Walsh and M. G. Kong, Appl. Phys. Lett. **91**, 251504 (2007).
[11]T. E. Nitschke and D. B. Graves, J. Appl. Phys. **76**, 5646 (1994).
[12]W. L. Shang, D. Z. Wang, and M. G. Kong, Astrophys. J. **16**, 1 (2007).
[13]M. Surendra and D. B. Graves, IEEE Trans. Plasma Sci. **19**, 144 (1991).
[14]D. Vender and R. W. Boswell, IEEE Trans. Plasma Sci. **18**, 725 (1990).
[15]M. Surendra, D. B. Graves, and G. M. Jellum, Phys. Rev. A **41**, 1112 (1990).
[16]T. Ledig and B. Schröder, J. Phys. D **26**, 1080 (1992).
[17]G. E. Georghiou, R. Morrow, and A. C. Metaxas, J. Phys. D **34**, 200 (2001).
[18]A. Hallac, G. E. Georghiou, and A. C. Metaxas, J. Phys. D **36**, 2498 (2003).
[19]M. C. Wang and E. E. Kunhardt, Phys. Rev. A **15**, 2366 (1990).
[20]S. O. Macheret, M. N. Shneider, and R. B. Miles, IEEE Trans. Plasma Sci. **30**, 1301 (2002).
[21]S. O. Macheret, M. N. Shneider, and R. C. Murray, Phys. Plasmas **13**, 130235 (2006).
[22]E. E. Kunhardt and Y. Tzeng, J. Comput. Phys. **67**, 279 (1986).
[23]Yu. P. Raizer and M. N. Shneider, High Temp. **27**, 329 (1989).
[24]T. H. Ahn, K. Nakamura, and H. Sugai, Plasma Sources Sci. Technol. **5**, 139 (1996).
[25]J. P. Boeuf and E. Marode, J. Phys. D **15**, 2169 (1982).